Electronic Spectra of Pyrazolyl-Bridged Binuclear Iridium(I) Complexes

Janet L. Marshall, Michael D. Hopkins,† Vincent M. Miskowski,* and Harry B. Gray*

Arthur Amos Noyes Laboratory,‡ California Institute of Technology, Pasadena, California 91125

Received May 4, 1992

The electronic absorption and emission spectra and emission lifetimes of $Ir_2(\mu\text{-}L)_2(CO)_4$ (L = pyrazolyl, 3-methylpyrazolyl, 3,5-dimethylpyrazolyl) have been determined in the temperature range 77–300 K. Polarized emission excitation spectra of the complexes in rigid glassy solutions at 77 K are also reported. Like face-to-face d^8–d^8 systems, these A-frame complexes display dipole-allowed transitions to emissive singlet and triplet excited states derived from monomer $d_{z^2} \rightarrow p_z$ excitations; these dimer excited states are stabilized relative to monomer excited states by strong metal–metal bonding. There is a second singlet/triplet pair of excited states, also derived from monomer $d_{z^2} \rightarrow p_z$ excitations; although transitions to these states are dipole forbidden in face-to-face structures, the corresponding bands in the absorption spectra of the A-frame complexes possess considerable intensity. These latter excited states have negligible metal–metal bonding stabilization relative to the monomer states, but considerable metal–ligand charge-transfer character, as judged by well-resolved ν(Ir–CO) vibronic structure in the absorption bands. Overall, the spectroscopic results are consistent with a valence-bond model for the Ir–Ir interaction.

Introduction

The electronic structures and photochemical and photophysical properties of face-to-face d^8–d^8 M_2L_8 complexes have been under investigation for many years.[1] It is now established that the lowest-energy excited states of most of these species are metal-localized $d\sigma^*(d_{z^2}) \rightarrow p\sigma(p_z)$ systems that are of lower energy than analogous monomer levels because of the strong metal–metal bonding associated with the $(d\sigma^*)^1(p\sigma)^1$ electronic configuration. Moreover, configuration interaction of the dimer d → p excited states with the ground state imparts weak metal–metal bonding to the latter.[1b]

Stobart and co-workers[2a,b] discovered a second important class of d^8–d^8 complexes, which is typified by the pyrazolyl-bridged species $M_2(\mu\text{-}L)_2L'_4$ (M = Ir(I), Rh(I); L′ = CO, alkene, phosphine; L = pyrazolyl (pz) or a substituted derivative thereof).[2,3] These molecules have a structure that is roughly an A-frame, consisting of two square-planar d^8 units tilted toward each other (limiting C_{2v} symmetry). The emission properties of these species closely resemble those of the face-to-face dimers in that both fluorescence and phosphorescence are observed;[4a,d,5] singlet and triplet $d\sigma^* \rightarrow p\sigma$ excited states have been respectively assigned as the sources of these emissions. The metal–metal distances vary considerably among these molecules; for example, $d(Ir_2)$ has been determined to be 3.506 Å for $Ir_2(\mu\text{-pz})_2(CO)_4$ and 3.245 Å for $Ir_2(\mu\text{-3,5-Me}_2\text{pz})_2(CO)_4$.[3] In addition, these compounds have shown interesting thermal[2,3] (particularly in regard to hydrogenation catalysis)[3] and excited-state[4] chemistry, with the A-frame structure likely being a significant factor in the reactivity patterns.

Detailed assignments of the electronic absorption spectra of this class of compounds have not been attempted until now. Complications associated with the low symmetry of the A-frame structure undoubtedly have inhibited progress in this area. However, advances in the understanding of the electronic spectra of face-to-face complexes,[1a] together with recently reported photoelectron spectroscopic data and theoretical studies of the pyrazolyl-bridged compounds,[6] have laid a foundation for assigning the transitions in the lower symmetry d^8–d^8 species. With the aid of polarized emission excitation spectra, we have been able to interpret the electronic absorption spectra of $Ir_2(\mu\text{-}L)_2L'_4$ complexes.

Experimental Section

Acetonitrile (Burdick and Jackson, UV grade) was freeze–pump–thaw-degassed and stored over alumina (Woelm N, Activity Grade 1) that had been activated by heating under dynamic vacuum ($<10^{-3}$ Torr) for 24 h. 2-Methylpentane (Phillips Petroleum) was refluxed over lithium aluminum hydride, degassed via several freeze–pump–thaw cycles, and vacuum-transferred to an evacuated storage flask containing lithium aluminum hydride. *n*-Hexane (Baker Reagent) was freeze–pump–thaw-

* To whom correspondence should be addressed.
† Present address: Department of Chemistry, University of Pittsburgh, Pittsburgh, PA 15260.
‡ Contribution No. 8535.

(1) (a) Smith, D. C.; Miskowski, V. M.; Mason, W. R.; Gray, H. B. *J. Am. Chem. Soc.* **1990**, *112*, 3759–3767. (b) Rice, S. F.; Miskowski, V. M.; Gray, H. B. *Inorg. Chem.* **1988**, *27*, 4704–4708. (c) Stiegman, A. E.; Rice, S. F.; Gray, H. B.; Miskowski, V. M. *Inorg. Chem.* **1987**, *26*, 1112–1116. (d) Rice, S. F.; Gray, H. B. *J. Am. Chem. Soc.* **1983**, *105*, 4571–4575. (e) Roundhill, D. M.; Gray, H. B.; Che, C.-M. *Acc. Chem. Res.* **1989**, *22*, 55.

(2) (a) Beveridge, K. A.; Bushnell, G. W.; Dixon, K. R.; Eadie, D. T.; Stobart, S. R.; Atwood, J. L.; Zaworotko, M. J. *J. Am. Chem. Soc.* **1982**, *104*, 920–922. (b) Coleman, A. W.; Eadie, D. T.; Stobart, S. R.; Zaworotko, M. J.; Atwood, J. L. *J. Am. Chem. Soc.* **1982**, *104*, 922–923. (c) Bushnell, G. W.; Fjeldsted, D. O. K.; Stobart, S. R.; Zaworotko, M. J. *J. Chem. Soc., Chem. Commun.* **1983**, 580–581. (d) Beveridge, K. A.; Bushnell, G. W.; Stobart, S. R.; Atwood, J. L.; Zaworotko, M. J. *Organometallics* **1983**, *2*, 1447–1451. (e) Bushnell, G. W.; Stobart, S. R.; Vefghi, R.; Zaworotko, M. J. *J. Chem. Soc., Chem. Commun.* **1984**, 282–284. (f) Atwood, J. L.; Beveridge, K. A.; Bushnell, G. W.; Dixon, K. R.; Eadie, D. T.; Stobart, S. R.; Zaworotko, M. J. *Inorg. Chem.* **1984**, *23*, 4050–4057. (g) Bushnell, G. W.; Fjeldsted, D. O. K.; Stobart, S. R.; Zaworotko, M. J.; Knox, S. A. R.; Macpherson, K. A. *Organometallics* **1985**, *4*, 1107–1114. (h) Bushnell, G. W.; Decker, M. J.; Eadie, D. T.; Stobart, S. R.; Vefghi, R.; Atwood, J. L.; Zaworotko, M. J. *Organometallics* **1985**, *4*, 2106–2111. (i) Fjeldsted, D. K. O.; Stobart, S. R. *J. Chem. Soc., Chem. Commun.* **1985**, 908–909. (j) Fjeldsted, D. K. O.; Stobart, S. R. *J. Am. Chem. Soc.* **1985**, *107*, 8258–8259. (k) Harrison, D. G.; Stobart, S. R. *J. Chem. Soc., Chem. Commun.* **1986**, 285–286. (l) Brost, R. D.; Fjeldsted, D. K. O.; Stobart, S. R. *J. Chem. Soc., Chem. Commun.* **1989**, 488–490. (m) Brost, R. D.; Stobart, S. R. *J. Chem. Soc., Chem. Commun.* **1989**, 498–500. (n) Brost, R. D.; Stobart, S. R. *Inorg. Chem.* **1989**, *28*, 4307–4308.

(3) Nussbaum, S.; Rettig, S. J.; Stoor, A.; Trotter, J. *Can. J. Chem.* **1985**, *63*, 692–702.

(4) (a) Marshall, J. L.; Stobart, S. R.; Gray, H. B. *J. Am. Chem. Soc.* **1984**, *106*, 3027–3029. (b) Caspar, J. V.; Gray, H. B. *J. Am. Chem. Soc.* **1984**, *106*, 3029–3030. (c) Marshall, J. L.; Stiegman, A. E.; Gray, H. B. *ACS Symp. Ser.* **1986**, *307*, 166–176. (d) Winkler, J. R.; Marshall, J. L.; Netzel, T. L.; Gray, H. B. *J. Am. Chem. Soc.* **1986**, *108*, 2263–2266. (e) Fox, L. S.; Marshall, J. L.; Gray, H. B.; Winkler, J. R. *J. Am. Chem. Soc.* **1987**, *109*, 6901–6902. (f) Fox, L. S.; Kozik, M.; Winkler, J. R.; Gray, H. B. *Science* **1990**, *247*, 1069–1071.

(5) Rodman, G. S.; Daws, C. A.; Mann, K. R. *Inorg. Chem.* **1988**, *27*, 3347–3353.

(6) Lichtenberger, D. L.; Copenhaver, A. S.; Gray, H. B.; Marshall, J. L.; Hopkins, M. D. *Inorg. Chem.* **1988**, *27*, 4488–4493.

0020-1669/92/1331-5034$03.00/0

degassed but otherwise used as received. Tetrahydrofuran (EM Science) was distilled under nitrogen from calcium hydride prior to use. Carbon monoxide (Matheson), carbon-13 monoxide (Monsanto, 99%), and 3-methylpyrazole (Aldrich, 97%) were used as received. The compounds $[Ir(COD)Cl]_2$[7] (COD = 1,5-cyclooctadiene), $Ir_2(\mu\text{-pz})_2(COD)_2$,[2a,f] $Ir_2(\mu\text{-}3,5\text{-}Me_2pz)_2(COD)_2$,[2g] and $Ir_2(\mu\text{-pz})_2(CO)_4$ (**3**)[3] were prepared according to previously described methods; these and the other syntheses described herein were carried out using standard Schlenk techniques. ^1H NMR spectra were recorded at 400 MHz on a JEOL GX-400 spectrometer. Procedures and equipment for electronic absorption and emission measurements have been described previously.[8] Procedures for polarized emission measurements have been given in detail,[8c] and only a brief description is presented here. Polarized excitation spectra were collected as four digital data files, $I_{ij}(\lambda_{ex})$, where the indices i and j refer to the excitation and emission polarizers, respectively, and have values of either v (vertical) or h (horizontal) in our 90° emission geometry. The emission polarization ratio is defined as $N = I_{\parallel}/I_{\perp} = (I_{vv}/I_{vh})(I_{hh}/I_{hv})$, where the second term in parentheses is a correction for nonideal spectrometer effects.[9] Since this term is found to be wavelength independent for our apparatus in the 230–700-nm range, it is also reasonable to define corrected values of $I_{\parallel} = I_{vv}(I_{hh}/I_{hv})$ and $I_{\perp} = I_{vh}$, and we present some of our data in this fashion. Note that other commonly used measures of polarization, such as the degree of polarization (P), are related[9] to N; e.g., $P = (N-1)/(N+1)$.

$Ir_2(\mu\text{-}3,5\text{-}Me_2pz)_2(CO)_4$ (1). Carbon monoxide was bubbled through a tetrahydrofuran solution (100 mL) of $Ir_2(\mu\text{-}3,5\text{-}Me_2pz)_2(COD)_2$ (0.925 g, 1.17 mmol) for 8 h at room temperature, during which time the initial purple solution turned orange. The solvent was removed under vacuum, and the residue was dissolved in *n*-hexane. Partial evaporation of the filtered extract with gentle heating (45 °C) gave a saturated solution, which was refrigerated for 24 h to yield large orange crystals of the product. These were removed by filtration, washed with ice-cold hexane, and dried under vacuum. Reduction of volume of the mother liquor under a stream of argon yielded a second crop of smaller crystals. Yield: 0.660 g (82%). Anal. Calcd (found) for $C_{14}H_{14}N_4O_4Ir_2$: C, 24.49 (24.50); H, 2.05 (2.09); N, 8.16 (8.24). ^1H NMR (acetone-d_6): δ 6.10 (s, 1, 4-H), 2.35 (s, 6, 3,5-CH_3).

$Ir_2(\mu\text{-}3\text{-}Mepz)_2(CO)_4$ (2). $[Ir(COD)Cl]_2$ (0.300 g, 0.447 mmol) was dissolved in tetrahydrofuran (30 mL) to give an orange-red solution. Excess triethylamine (0.25 mL, 1.8 mmol) and 3-methylpyrazole (0.080 mL, 0.994 mmol) were added against an argon counterflow. After 20 h, a solid had precipitated from the purple solution. The solvent was removed under vacuum, and the residue was extracted with benzene (50 mL). The extract was filtered, and the solvent was removed. The residue was dissolved in tetrahydrofuran (50 mL), and CO was bubbled through the solution for 2 h. The resulting yellow-orange solution was evaporated to dryness under vacuum and extracted with acetonitrile (40 mL). Slow evaporation under a stream of argon yielded the product as an air-stable, yellow, crystalline material, which was washed with ice-cold acetonitrile (2 mL) and vacuum-dried. Yield: 0.210 g (71%). Anal. Calcd (found) for $C_{12}H_{10}N_4O_4Ir_2$: C, 21.88 (22.08); H, 1.53 (1.55); N, 8.51 (8.51). ^1H NMR (acetone-d_6): δ 7.72 (d, 1,5-H), 7.71 (d, 1,5-H), 6.31 (m, 2,4-H), 2.42 (s, 3,3-CH_3), 2.41 (s, 3,3-CH_3). The observation of two resonances each for the 3-CH_3 and 5-H nuclei presumably reflects the presence of two isomers in nearly equal amounts.

$Ir_2(\mu\text{-pz})_2(^{13}CO)_4$. The ^{13}C-labeled complex was prepared on a high-vacuum line by blanketing a dilute 2-methylpentane solution of $Ir_2(\mu\text{-pz})_2(COD)_2$ in a spectrophotometric cell with ^{13}CO. The exchange of COD for CO was complete upon mixing, as evidenced by the electronic absorption spectrum.

Results and Discussion

Monomer and Dimer Model Systems. The symmetry axes employed here are shown in Figure 1. For *cis*-$IrX_2L_2^-$ we retain the usual orbital designations (e.g., d_{z^2}) of planar four-coordinate complexes by exchanging the conventional x and z axes of the

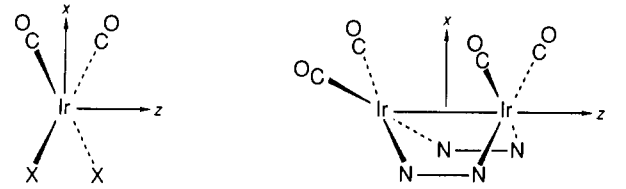

Figure 1. Symmetry axes for mono- and binuclear Ir(I) complexes. In each case, the x axis is taken as the C_2 axis in C_{2v} symmetry.

Table I. Electronic Transition Assignments for Monomeric Complexes[a]

D_{4h} assignt $^1A_{1g} \rightarrow$	complex: $Ir(CN\text{-}t\text{-}Bu)_4^+$ [b]	complex: *cis*-$Ir(CN)_2(CO)_2^-$ [c]	complex: *cis*-$IrCl_2(CO)_2^-$ [c]
$E_u(^3A_{2u})$ ($d_{z^2} \rightarrow p_z$)	489 (870)	461 (570)	385 (530)
$A_{2u}(^1A_{2u})$ ($d_{z^2} \rightarrow p_z$)	423 (4100)	402 (2960)	351 (2380)
$E_u(^3E_u)$ ($d_{xz,yz} \rightarrow p_z$)	373 (5900)	346 (1980)	316 (2040)
$E_u(^1E_u)$ ($d_{xz,yz} \rightarrow p_z$)	308 (14500)	290 (5030)	259 (4700)
$E_u(^3B_{1u})$[d] ($d_{x^2-y^2} \rightarrow p_z$)	291 (5500)	278 (4450 sh)	236 (4200)

[a] Entries have the form λ_{max}/nm (ϵ_{max}/M^{-1} cm^{-1}). [b] Reference 1a. [c] Reference 10b. [d] Designation assumes molecular x and y axes bisect the metal–ligand axes (Figure 1).

C_{2v} point group; thus, the C_2 axis is the x axis. A face-to-face dimer formed from these fragments then conforms to the standard convention of a metal–metal z axis. The A-frame structure of the complexes (Figure 1) is formed by tilting the square-planar units away from each other in such a way as to maintain x as the C_2 axis.

Our choice of axes results in the $d_{z^2} \rightarrow p_z$ transition of the monomer transforming as B_1 in the C_{2v} point group, in accord with the conventions adopted in discussions of monomer spectra,[10] as well as with the symmetry designations used in the theoretical calculations on $Ir_2(\mu\text{-pz})_2(CO)_4$ complexes.[6] For clarity with regard to comparison to other work,[4a-d] we note that an exchange of the x and y axes exchanges the B_1 and B_2 state and orbital labels.

Selected electronic spectroscopic data for monomeric Ir(I) complexes are set out in Table I. We choose $Ir(CN\text{-}t\text{-}Bu)_4^+$ (D_{4h} symmetry) as a starting point because its electronic absorption spectrum is well understood.[1a,10] The various electronic transitions are assigned as metal-localized $d \rightarrow p_z$ excitations, with the understanding that there is mixing between the metal p_z and ligand π^* orbitals. The lowest two bands are due to excitations to triplet and singlet $d_{z^2} \rightarrow p_z$ excited states, while three higher-energy bands arise from $d\pi(d_{xz,yz,x^2-y^2}) \rightarrow p_z$ excitations that correspond to excited states of E_u symmetry. There are large spin–orbit interactions among the latter states,[1,10] so the assignments to specific singlet or triplet transitions (Table I) are simplifications. The $d\pi \rightarrow p_z$ excitations also give rise to a number of excited states of symmetries other than E_u, but bands associated with transitions to these states are all relatively weak.[1b]

The spectrum of the related C_{2v}-symmetry *cis*-$Ir(CN)_2(CO)_2^-$ ion is strictly analogous: there are shifts of all absorptions to higher energy by 1200–2100 cm^{-1} and a broadening of the higher energy bands that possibly indicates a slight lifting of the (x,y)-degeneracy of D_{4h} symmetry. Replacement of CN^- by Cl^- results in an additional shift of the bands to higher energy by 2700–6500 cm^{-1}. This is likely attributable[10] to the sensitivity of the p_z orbital energy to the π-donor/acceptor nature of the ligands: p_z is stabilized by mixing with the π^* orbitals of acceptor ligands such

(7) Herde, J. L.; Lambert, J. C.; Senoff, C. V. *Inorg. Synth.* **1974**, *15*, 18–20.
(8) (a) Hopkins, M. D.; Schaefer, W. P.; Bronikowski, M. J.; Woodruff, W. H.; Miskowski, V. M.; Dallinger, R. F.; Gray, H. B. *J. Am. Chem. Soc.* **1987**, *109*, 408–416. (b) Hopkins, M. D.; Miskowski, V. M.; Gray, H. B. *J. Am. Chem. Soc.* **1988**, *110*, 1787–1793. (c) Miskowski, V. M.; Gray, H. B.; Hopkins, M. D. *Inorg. Chem.* **1992**, *31*, 2085.
(9) Lakowicz, J. R. *Principles of Fluorescence Spectroscopy*; Plenum Press: New York, 1983.
(10) (a) Brady, R.; Flynn, B. R.; Geoffroy, G. L.; Gray, H. B.; Peone, J., Jr.; Vaska, L. *Inorg. Chem.* **1976**, *15*, 1485–1488. (b) Geoffroy, G. L.; Isci, H.; Litrenti, J.; Mason, W. R. *Inorg. Chem.* **1977**, *16*, 1950–1955.

as CO, CN^-, and RNC, whereas chloride, which is a π donor, results in the destabilization of p_z relative to the other ligand sets.

The large π-bonding asymmetry in *cis*-$IrCl_2(CO)_2^-$ also could lead to large $d_{xz,yz}$ splittings, and hence splittings of the E_u (D_{4h} symmetry) excited states. This is not observed in the absorption spectrum, although MCD data[10b] do suggest modest splittings of the E_u states.

We propose to employ *cis*-$IrCl_2(CO)_2^-$ and closely related compounds[10b] as monomeric spectroscopic models for $Ir_2(\mu\text{-pz})_2(CO)_4$ and its ring-methylated analogues. Electronic structure calculations indicate that the bridging pyrazolyl ligands do not engage in π back-bonding.[6] Rather, these ligands are good σ donors and weak π donors.

The spectroscopic consequences of the formation of a face-to-face dimer of $Ir(CNR)_4^+$ have been examined in detail in terms of a valence-bond (VB) model.[1a] Key findings are that a pair of excited states (singlet and triplet), correlating to the monomer $d_{z^2} \rightarrow p_z$ excitation, are strongly stabilized, whereas transitions corresponding to monomer $d\pi \rightarrow p_z$ excitations are little perturbed. There are, in addition, metal–metal charge-transfer excitations, such as $d_{z^2}(Ir(1)) \rightarrow p_z(Ir(2))$ that fall at much higher energies.[1a] The VB model starts with dipole–dipole coupling of the monomer excitations, yielding in-phase and out-of-phase combinations (where the phase refers to the molecular $z(Ir_2)$ axis). The Davydov splitting of the monomer excitations resulting from dipole–dipole coupling is expected to be small[11] for these moderately intense (oscillator strength ca. 0.1) electronic transitions because of the large metal–metal distances of these species (3.0–3.5 Å). This is consistent with the small perturbations observed for the $d\pi \rightarrow p_z$ transitions upon dimer formation. For a face-to-face dimer, the in-phase combination of $d_{z^2} \rightarrow p_z$ monomer transitions carries all of the intensity. The large stabilizations observed for these transitions are explained in the context of the VB model by the fact that these excited states can collapse to strongly metal–metal-bonded $d\sigma^* \rightarrow p\sigma$ "molecular orbital" excited states upon reduction of the metal–metal distance. The out-of-phase $d_{z^2} \rightarrow p_z$ combinations ($^1A_{1g} \rightarrow {}^{1,3}A_{1g}$ in D_{4h}) are dipole forbidden, although very weak absorption bands corresponding to these excitations have been identified in low-temperature single-crystal spectra.[1a,b] Like the $d\pi \rightarrow p_z$ excitations, they are little shifted from the monomer excitations, which is consistent with the VB model.[1a]

Electronic Absorption Spectra of $Ir_2(\mu\text{-L})_2(CO)_4$. Room-temperature electronic absorption spectra of $Ir_2(\mu\text{-3,5-Me}_2\text{pz})_2(CO)_4$ (**1**), $Ir_2(\mu\text{-3-Mepz})_2(CO)_4$ (**2**), and $Ir_2(\mu\text{-pz})_2(CO)_4$ (**3**) are shown in Figure 2, and the data are set out in Table II. We do not report spectra for $\lambda < 300$ nm, because there are pyrazolyl-localized absorptions in this region, complicating the interpretation.

The spectra are similar to those previously reported for analogues in which two to four of the CO ligands are replaced by phosphines or alkenes.[4a,e] There is an intense low-energy band for these species, labeled B in Table II, that is red-shifted with respect to intense monomer bands (Table I) of *cis*-$IrCl_2(CO)_2^-$; we assign this band to the $^1A_1 \rightarrow {}^1B_1$ $^1(d\sigma^* \rightarrow p\sigma)$ transition. The band shifts to higher energy according to **1** < **2** < **3**, which is the order of increasing metal–metal bond length (assuming that the distance for **2** is intermediate to those of **1** and **3**),[3] and concomitantly decreases in intensity. Spectra at 77 K (Figure 3) reveal an additional weak band (A) to lower energy of band B. Both the intensity of band A and its red shift from band B, ca. 2500 cm^{-1} for all three compounds, are consistent[1] with assignment to $^1A_1 \rightarrow {}^3B_1$ ($d\sigma^* \rightarrow p\sigma$).

The energies and intensities of the bands observed at $\lambda < 380$ nm (bands E and F) suggest that they are analogous to $d\pi \rightarrow p_z$ transitions of monomer analogues (Table I). A specific assignment consistent with the spectrum of *cis*-$Ir_2Cl_2(CO)_2^-$ is that E and F are the two C_{2v}-symmetry components of the D_{4h}-symmetry $^1A_{1g} \rightarrow E_u(^3E_u)$ $d_{xz,yz} \rightarrow p_z$ transition; the inferred $d_{xz,yz}$ splitting of ca. 3000 cm^{-1} is in agreement with electronic structure calculations.[6] Additionally consistent with this assignment is that bands E and F blue-shift along the series **1**–**3**, since the photoelectron data[6] indicate considerable destabilization of $d\pi$ levels upon methylation of the pyrazolyl ligands.

Bands C and D, on the other hand, bear little resemblance to features seen in the monomer spectra or to any bands reported for face-to-face dimers; they are quite difficult to ignore, moreover, in that they are distinctly vibronically structured in quanta of 490 (±20) cm^{-1}. It is noteworthy that vibronic structure is even evident at room temperature (Figure 1). In the case of **3**, we also determined the 77 K absorption spectrum of the ^{13}CO derivative. The observation that the vibronic spacing is reduced to 470 (±20) cm^{-1}, as expected for an Ir–(CO) oscillator, indicates the vibrational mode to be ν(Ir–CO); the frequency is much too high

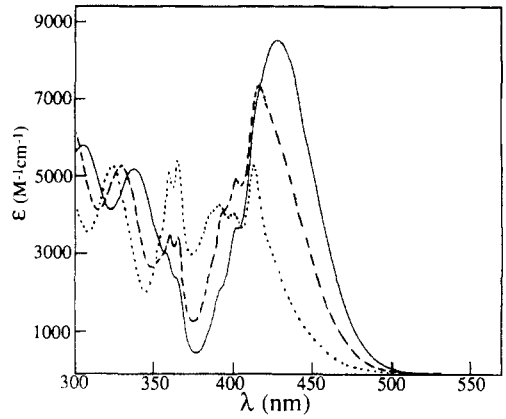

Figure 2. Electronic absorption spectra of **1** (—), **2** (- - -), and **3** (···) in 2-methylpentane solution at room temperature.

Table II. Electronic Absorption Data for $Ir_2(\mu\text{-L})_2(CO)_4$ Complexes in 2-Methylpentane Solution at Room Temperature[a]

band designation	assignt	1	2	3
A	$d_{z^2} \rightarrow p_z$ $^1A_1 \rightarrow A_1,B_2$ ($^3B_1$)	470 sh[b]	455 sh[b]	~440 sh[b]
B	$d_{z^2} \rightarrow p_z$ $^1A_1 \rightarrow B_1$ ($^1B_1$)	426 (8500)	412 (7400)	390 (4300)
C	$d_{z^2} \rightarrow p_z$ $^1A_1 \rightarrow B_1$ ($^3A_1$)	401 (3750)	399 (5030)	410 (5350)
D	$d_{z^2} \rightarrow p_z$ $^1A_1 \rightarrow A_1$ ($^1A_1$)	364 (2300)	364 (4450)	363 (5550)
E	$d\pi \rightarrow p_z$	336 (5150)	328 (5250)	322 (5250)
F	$d\pi \rightarrow p_z$	305 (5800)	<300	<300

[a] Entries are in the form λ_{max}/nm (ϵ_{max}/M^{-1} cm^{-1}). [b] Not resolved at room temperature. Reported wavelengths are those observed at 77 K (ϵ < 1000).

(11) Consider a symmetrical dimer oriented as in Figure 11. A single-axis-polarized, dipole-allowed electronic transition of the monomer undergoes a dipole–dipole induced energetic splitting that is given according to first-order perturbation theory[12] by

$$\Delta W = 2e^2|D|^2R^{-3}(1 + \cos^2\theta) \quad (1)$$

where e is the electronic charge, D is the monomer transition dipole moment (with conventional units of length), R is the metal–metal distance, and θ is defined in Figure 11. For an estimate of $|D|^2$ for the singlet–singlet $d_{z^2} \rightarrow p_z$ transition of an Ir(I) monomer, we turn to the well-studied complex[1a] $Ir(CN\text{-}t\text{-}Bu)_4^+$, which has an oscillator strength and an energy of 0.021 and 23 640 cm^{-1}, respectively. We then calculate a value of $|D|^2 = 0.082$ Å^2. Rough calculations of $|D|^2$ for other Ir(I) monomers based on literature data[10] give estimates that agree with this one to within a factor of 2. With this value and values of R and θ appropriate for compounds **1** and **3**, eq 1 gives estimates of ΔW of respectively 630 and 905 cm^{-1}. For comparison to these values, the calculated splitting for a face-to-face dimer with $R = 3.25$ Å is 1100 cm^{-1}.

(12) (a) Craig, D. P.; Walmsley, S. H. *Excitons in Molecular Crystals*; Benjamin: New York, 1968. (b) Philpott, M. R. *Adv. Chem. Phys.* **1973**, *23*, 227–341.

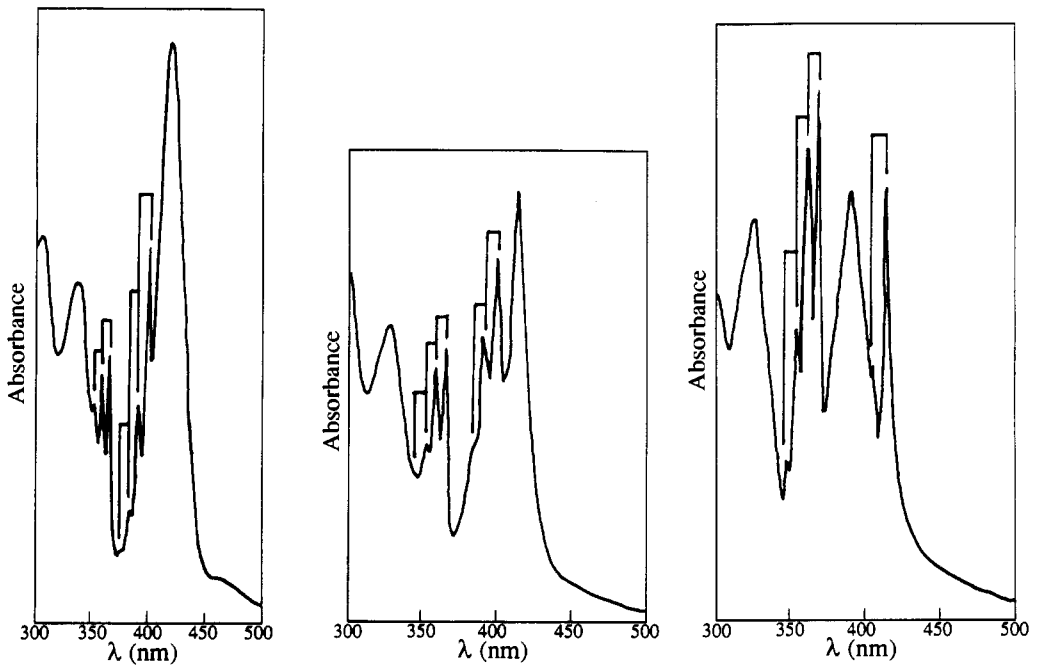

Figure 3. Electronic absorption spectra in 2-methylpentane solution at 77 K: (a, left) **1**; (b, middle) **2**; (c, right) **3**. Vibronic progressions in ν(Ir-(CO)) are indicated.

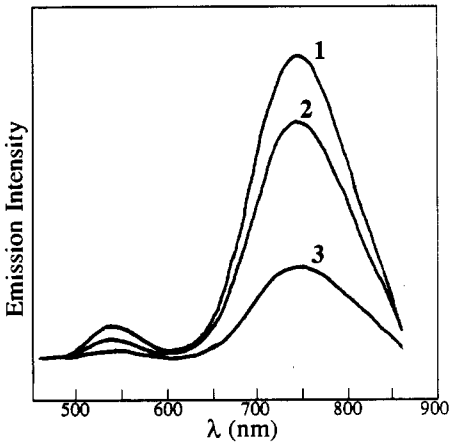

Figure 4. Corrected emission spectra (436-nm excitation) of **1**–**3** in 2-methylpentane solution at room temperature. Relative intensities roughly scale with the phosphorescence quantum yield.

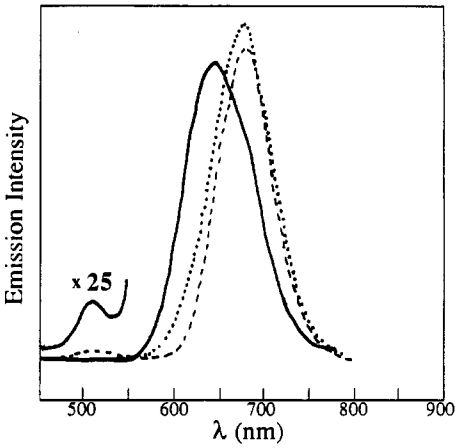

Figure 5. Corrected emission spectra (436-nm excitation) at 77 K in 2-methylpentane solution of **1** (—), **2** (- - -), and **3** (···).

to be $\nu(Ir_2)$.[1a] The 0–0 transitions of bands C and D do not shift for the ^{13}CO derivative, however, indicating that the spacing between them cannot correspond to one quantum of ν(CO). Bands C and D are thus due to two distinct but very similar electronic transitions. Finally, we note that band C and, to a lesser extent, band D intensify along the series **1**–**3** but shift very little in energy.

Emission Properties. Emission spectra for compounds **1**–**3** at room temperature are shown in Figure 4, and spectra at 77 K are shown in Figure 5; photophysical parameters are summarized in Table III. Fluorescence lifetimes have not been measured for these compounds. Given the small room-temperature fluorescence quantum yields ($(1–5) \times 10^{-3}$), fluorescence lifetimes are probably of the order of 100 ps, similar to those reported for several phosphine-substituted analogues[4f] that have comparable fluorescence quantum yields. The compound $Ir_2(\mu\text{-pz})_2(COD)_2$ has a shorter singlet lifetime (<20 ps)[4d] and lower fluorescence quantum yield (10^{-4}),[4a] and low fluorescence yields are generally observed for a variety of $Ir_2(\mu\text{-L})_2(COD)_2$ complexes,[5,13a] along with relatively short triplet lifetimes at room temperature (250 ns for $Ir_2(\mu\text{-pz})_2(COD)_2$). The enhancement of nonradiative decay rates of the $^{1,3}B_1$ states of COD derivatives is not presently understood.

Table III. Photophysical Parameters for $Ir_2(\mu\text{-L})_2(CO)_4$ in 2-Methylpentane Solution at 300 and 77 K[a]

complex	emission λ_{max}, nm		Φ_{em}		τ, μs
	$^1B_1$	$^3B_1$	$^1B_1$	$^3B_1$	$^3B_1$
1	535 (505)	740 (675)	0.0051	0.096	3.3 (10.9)
2	537 (505)	742 (673)	0.0035	0.079	0.58 (10.2)
3	540 (505)	743 (640)	0.0014	0.032	0.35 (10.2)

[a] Values at 77 K in parentheses.

The emissions at both 300 and 77 K exhibit shifts along the series **1**–**3** that are much smaller than those of the corresponding absorption bands. A qualitative explanation for this phenomenon derives from the fact that the $d\sigma^* \rightarrow p\sigma$ excited states have considerably shorter metal–metal distances than the ground state (Figure 6).[1] Assuming that the excited-state metal–metal distance will be largely determined by the strong metal–metal bonding of the $d\sigma^* \rightarrow p\sigma$ state, the excited states of the various compounds should have similar potential surfaces. This is in contrast to the ground states, where very weak metal–metal bonding results in the metal–metal equilibrium distance being extremely sensitive

(13) (a) Marshall, J. L. Ph.D. Thesis, California Institute of Technology, 1986. (b) Fox, L. S. Ph.D. Thesis, California Institute of Technology, 1989.

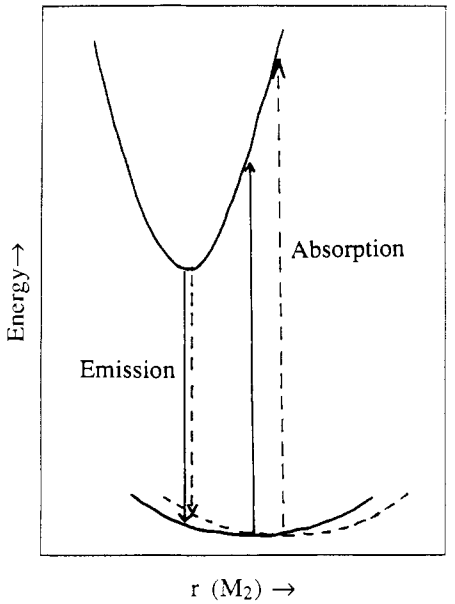

Figure 6. Semiquantitative potential energy surfaces for $d\sigma^* \rightarrow p\sigma$ excitations, calculated on the basis of the observed ground- and excited-state force constants and metal–metal distances given in ref 1b. The disparate effect of variation in ground-state equilibrium distance upon the emission and absorption vertical transitions is indicated by showing shifted ground-state potential surfaces for two different metal–metal distances.

to perturbations such as pyrazolyl-ring substitution, as evidenced by the structural data.[3] Since the ground-state potential surface will be broader than the excited-state surface, changes in ground-state equilibrium distance will have much larger effects on the vertical absorption energies than on vertical emission energies (Figure 6).

In contrast to the absorption maxima of these compounds, which are relatively insensitive to temperature, substantial shifts occur in the emission maxima of **1–3** between 300 and 77 K. However, much of the shift occurs near 120 K, which is in the glass-transition region of 2-methylpentane. Rigidochromic effects of this sort, including changes in emission lifetimes in the glass-transition temperature region, have been noted for other $Ir_2(\mu\text{-}L)_2L'_4$ complexes,[5,13b] although not for face-to-face d^8–d^8 species.[14] The A-frame geometry of the former apparently makes their relaxed excited-state geometry sensitive to the rigidity of the environment.

The fluorescence quantum yields of **1–3** are only weakly temperature dependent, but phosphorescence yields increase dramatically at lower temperatures. The quantum yields scale with the emission lifetimes, so a temperature-dependent nonradiative decay process is involved, as has also been noted for other d^8–d^8 systems.[5,13,14] Arrhenius plots of the phosphorescence lifetimes in the fluid region of 2-methylpentane yield activation energies (E_a) of 1300, 550, and 650 cm^{-1} for **1–3**, respectively, with preexponential factors (A) of ca. 10^8 s^{-1}. These parameters are substantially different from those reported[5,15] for $Ir_2(\mu\text{-}pz)_2(COD)_2$ (E_a = 4467 cm^{-1}, $A = 2.8 \times 10^{11}$ s^{-1}). We do not understand these differences at present.

A final point of interest is that the shape of the fluorescence band of **3** is similar to that of the other compounds, despite the fact that the maximum of band C has dropped below that of band B for this compound (Figure 3c). Evidently, the electronic origin

(14) (a) Rice, S. F.; Milder, S. J.; Gray, H. B.; Goldbeck, R. A.; Kliger, D. S. *Coord. Chem. Rev.* **1982**, *43*, 349–354. (b) Milder, S. J. *Inorg. Chem.* **1985**, *24*, 3376–3378. (c) Miskowski, V. M.; Milder, S. J.; Rice, S. F.; Gray, H. B. To be submitted for publication.

(15) Reference 4a reports 2600 cm^{-1} for the activation energy of $Ir_2(\mu\text{-}pz)_2(COD)_2$. The substantial difference from the value of ref 5 presumably results from differences in data treatment.

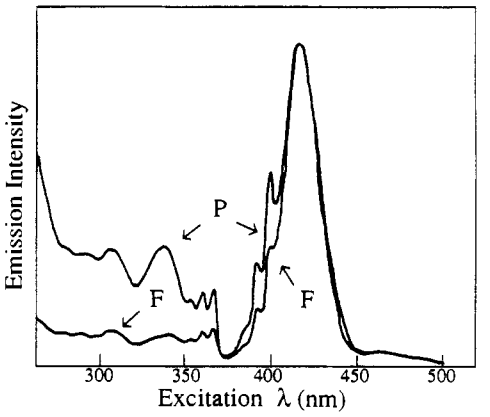

Figure 7. Corrected unpolarized fluorescence (F, $^1B_1 \rightarrow {}^1A_1$) and phosphorescence (P, $^3B_1 \rightarrow {}^1A_1$) excitation spectra of **1** in 2-methylpentane glass at 77 K, normalized at 417 nm.

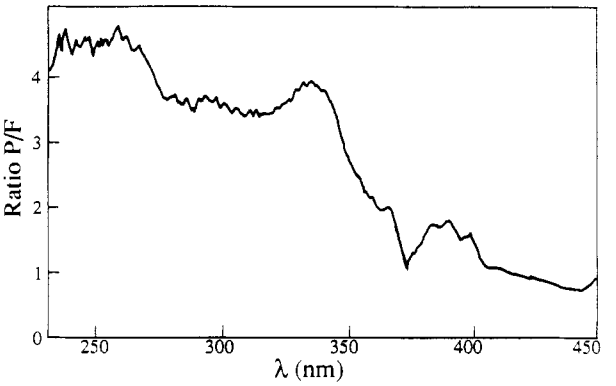

Figure 8. Ratio of the phosphorescence/fluorescence excitation spectra (P/F, Figure 7) normalized at 417 nm.

of band B still lies lower in energy than that of band C; band B is relatively broad, since it is due to a transition to an excited state that has an Ir_2 distance considerably different from that of the ground state.

Emission Excitation Spectra. Corrected fluorescence and phosphorescence excitation spectra of **1** in 2-methylpentane at 77 K are shown in Figure 7. The phosphorescence excitation spectrum agrees reasonably well with the 77 K absorption spectrum (Figure 3a) down to 300 nm. Below this wavelength, the phosphorescence yield seems to decrease, perhaps because absorption is in part into pyrazolyl-localized states that may not efficiently transfer energy to the emissive metal–metal states.

The fluorescence excitation spectrum shows that the various absorption bands above band B ($^1A_1 \rightarrow {}^1B_1$) all yield fluorescence relatively inefficiently. This phenomenon has been previously noted[13b] for other $Ir_2(\mu\text{-}L)_2L'_4$ complexes, as well as for face-to-face dimers.[14b,c] It is attributable to direct nonradiative decay of the upper excited states to the lowest triplet excited state, bypassing the fluorescent singlet excited state.

The ratio of the fluorescence and phosphorescence excitation spectra of **1**, normalized to the 417-nm maximum of band B at 77 K, is shown in Figure 8. The absorptions below 350 nm all show normalized ratios of 3.5–4.5; thus, neglecting any other energy-loss processes, internal-conversion efficiencies to $^1B_1$ are about 20–30%, which are similar to those observed for $d\pi \rightarrow p_z$ excited states of other d^8–d^8 dimers.[14b,c] Bands C and D possess conversion efficiencies near 50%, which suggest that they are relatively strongly coupled to the $^1B_1$ fluorescent state.

Polarized "photoselection" fluorescence excitation data for **1** are illustrated in Figure 9. The weakness of the fluorescence made this measurement very difficult with our apparatus, and the signal/noise ratio is low. The polarization ratio (N) for excitation directly into the $^1A_1 \rightarrow {}^1B_1$ absorption is 1.8–1.9.

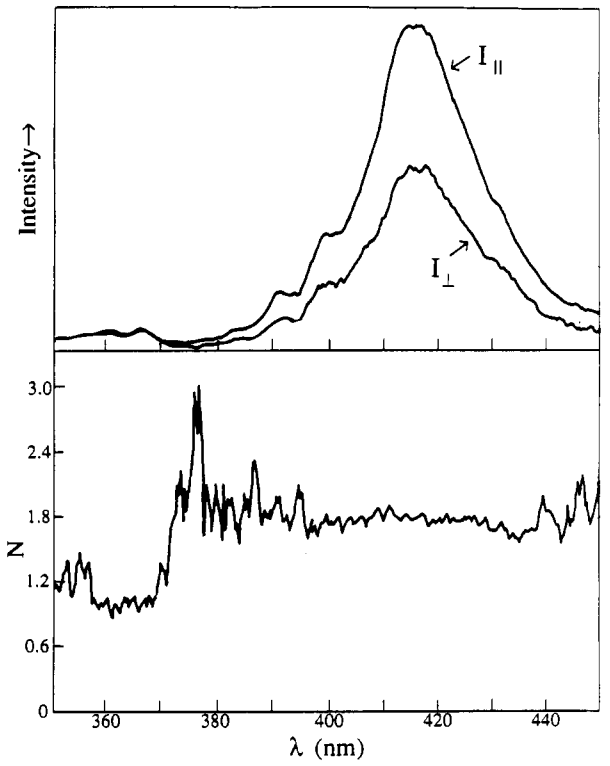

Figure 9. Corrected polarized excitation spectra for the $^1B_1 \rightarrow {}^1A_1$ fluorescence of **1** in 2-methylpentane glass at 77 K. Shown are $I_{\parallel}$, $I_{\perp}$, and $N = I_{\parallel}/I_{\perp}$.

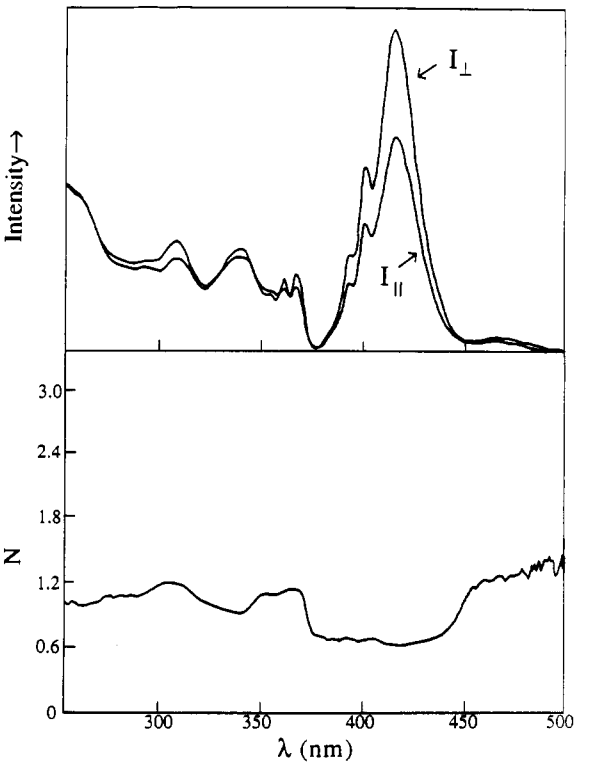

Figure 10. Corrected polarized excitation spectra for $^3B_1 \rightarrow {}^1A_1$ phosphorescence of **1** in 2-methylpentane glass at 77 K. Shown are $I_{\parallel}$, $I_{\perp}$, and $N = I_{\parallel}/I_{\perp}$.

Theoretical values[9] of N for emission and absorption polarized along the same single axis and for emission and absorption polarized perpendicular to each other are $N = 3$ and $N = 0.5$, respectively; employing our apparatus with high-quality glassy samples, we typically observe experimental values of N equal to 1.9–2.4 for the former case and 0.6–0.7 for the latter,[8c] the experimental loss of polarization resulting largely from sample imperfections. The observed value of N for transitions between the $^1A_1$ and $^1B_1$ states is clearly consistent with expectation for $\|z$-polarized (Figure 1) absorption and emission.

The value of N drops drastically near 370 nm and remains <1 in this region. While our data in this region are extremely noisy, they are still consistent with all of these absorptions being polarized perpendicular to the $\|z$-polarized fluorescence, as expected for $d\pi \rightarrow p_z$ excitations. It is noteworthy, however, that N remains large and constant through the structured band C, right up to the onset of band D. We conclude that the polarization ratio of band C is the same as that of band B; that is, band C must be $\|z$-polarized. Band D, on the other hand, is $\perp z$-polarized.

Analogous polarization data for the $^3B_1 \rightarrow {}^1A_1$ phosphorescence excitation spectrum of **1** are shown in Figure 10. The $^3B_1$ state is split by spin–orbit coupling into states of A_1, B_2, and A_2 symmetries; the first two correlate to the D_{4h} $E_u(^3A_{2u})$ state of face-to-face dimers, transitions to the ground state from which are dipole-allowed with x and y polarizations, respectively (Figure 1). The transitions involving the A_2 component are dipole-forbidden, like those of the $A_{1u}(^3A_{2u})$ D_{4h} state to which it correlates.[1] Consistent with these considerations, N is <1 for excitation into band B ($^1A_1 \rightarrow {}^1B_1$) at 77 K and remains so for excitation into band C, again consistent with $\|z$ polarization.

More detailed analysis of Figure 10 requires consideration of the magnitude of the spin–orbit splitting of the $^3B_1$ state. Since N remains at ca. 1.3 for excitation across band A, the spin–orbit splitting is evidently sufficiently small compared to the bandwidth that we cannot selectively populate the A_1 and B_2 states by absorption, since large changes in N across the band would otherwise have been observed. This is as expected, since spin–orbit splittings of $^3(d\sigma^* \rightarrow p\sigma)$ states are generally observed to be quite small (e.g., 41 cm^{-1} for $Pt_2(H_2P_2O_5)_4^{4-}$).[1d,e] The observed value of N is consistent with the theoretical value of 4/3 when either absorption or emission involves an effectively degenerate transition, and the other process (emission or absorption), whether or not it is effectively degenerate, is polarized in the same plane.[9]

A separate but related question is whether the spin–orbit splitting of the $^3B_1$ state is large enough that the emission at 77 K is predominantly from one or another of the spin–orbit states, which would only require that the A_1,B_2 splitting be comparable to kT (54 cm^{-1} at 77 K). If this is true, and if the x,y splittings of any of the upper $d\pi \rightarrow p_z$ states are large (as a calculation[6] predicts to be the case), then excitations to these states should yield polarization ratios deviating from 4/3 toward either 3 or 0.5, depending upon whether the polarization of the absorption was parallel or perpendicular to the predominant (either x or y) emission. Moreover, as set out in the following section, there are theoretical reasons to believe that band D is purely $\|x$-polarized. In fact, we observe only very small variations in N (1.0–1.3) for excitation into bands D–F. We therefore think it likely that the $^3B_1$ spin–orbit splitting is small compared to kT at 77 K. Since the splitting of the A_1 and B_2 spin–orbit states arises only by second-order spin–orbit coupling to upper excited states of these symmetries, this is not unreasonable.

Assignment of Bands C and D. The energies of bands C and D are nearly constant for compounds **1**–**3**; thus, they appear to be independent of both alkylation of the bridging pyrazolyl ligand and of the ground-state Ir_2 distance. Furthermore, the energies of bands C and D are fairly close to those of the $d_{z^2} \rightarrow p_z$ ($^1A_1 \rightarrow {}^{1,3}B_2$) excitations of *cis*-$IrCl_2(CO)_2^-$ (Table I). However, the intensities of these bands vary greatly, both absolutely and relative to those of the other absorption bands of the dimers.

Let us examine a simple dipole–dipole coupling model for the intensities of weakly coupled monomer excitations in more detail. A $\|z$-polarized transition of a monomer yields, by simple vector addition, two dimer transitions. In C_{2v} symmetry, the ratio of the intensities of the out-of-phase (A_1 symmetry) and in-phase (B_2 symmetry) combinations is $I(A_1)/I(B_2) = \tan^2\theta$, where θ is defined in Figure 11. For a face-to-face dimer, θ is zero, and as stated

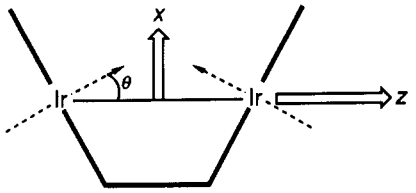

Figure 11. Schematic structural representation for an A-frame $Ir_2(\mu\text{-}L)_2L'_4$ complex, showing dipole–dipole coupling of perpendicular-to-plane polarized monomer transitions (moments shown as dashed arrows) to yield moments for two resultant transitions parallel to Ir–Ir (z) and perpendicular to Ir–Ir (x).

previously, the out-of-phase A_1(A_{1g} in D_{4h})-symmetry transition has no dipole-allowed intensity (although very weak transitions of this type have been observed[1a,b] in low-temperature single-crystal spectra). The crystal structures of **1** and **3** indicate θ = 38.1 and 48.7°, respectively,[3] corresponding to calculated values of $I(A_1)/I(B_2)$ = 0.615 and 1.30.

As noted earlier, a VB model for these excitations predicts that the out-of-phase $d_{z^2} \rightarrow p_z$ transitions will not be strongly perturbed from monomer excitations.[1a] This prediction is not modified by the tilting introduced by the A-frame structure. We therefore suggest that bands D and C are the out-of-phase excitations, $^1A_1 \rightarrow {}^1A_1$ and $^1A_1 \rightarrow {}^3A_1$, respectively. The former transition is dipole-allowed in $\|x$ polarization (Figure 1), as predicted by the dipole–dipole coupling model, and the relative intensities of bands D and B are in reasonable agreement with that predicted from $\tan^2\theta$.

This model cannot, however, explain the high intensity of band C, since the singlet–triplet excitation of the monomers has little intensity (Table I), as is consistent with the low intensity of band A. To explain the intensity of band C, we must consider spin–orbit coupling, which yields states of A_2, B_1, and B_2 symmetries from a $^3A_1$ state. Since for each of the compounds band C is near band B, we can expect that the $^1A_1 \rightarrow B_1$ ($^3A_1$) component will mix strongly with the $^1A_1 \rightarrow B_1$ ($^1B_1$) transition. This explains the identical polarizations of bands C and B and is consistent with the fact that the intensity of band C is highest for **2**, for which bands C and B occur at nearly the same energy. We note that the absence of singlet–triplet mixing of this type for face-to-face dimers[1] presumably reflects its symmetry-forbidden nature in D_{4h} symmetry; large spin–orbit mixing of the higher energy singlet and triplet $d\pi \rightarrow p_z$ type states, which is symmetry-allowed in D_{4h}, was observed for a face-to-face binuclear iridium complex.[1a]

The dipole–dipole coupling model also predicts[12] an energetic splitting of the in-phase and out-of-phase $d_{z^2} \rightarrow p_z$ combinations of the dimer. However, we calculate[11] this Davydov splitting to be considerably smaller than the observed value, so stabilization of the $^{1,3}B_1$ states via covalent metal–metal bonding is considered to be the major factor in determining the observed splittings. An additional reason in favor of this interpretation is that the dipole–dipole coupling model predicts much smaller splittings for the two triplet excitations, since the monomer excitation carries much less dipole strength, and this is contrary to observation.

Our assignments nicely explain the energies and intensities of bands C and D. However, their prominent vibronic structure in ν(Ir–CO) remains to be interpreted. As noted by others,[10] the ligand dependences of the monomer $d \rightarrow p_z$ excitations can be explained in terms of orbital mixing of ligand π^* with metal p_z. This amounts to mixing metal–ligand charge-transfer (MLCT) character into the excitations, and the vibronic progressions can be understood on the basis of this character. Franck–Condon simulations[16] of bands C and D yielded a value of $S = I(1,0)/I(0,0) = 0.7$, which corresponds to $\Delta Q = 0.06$ Å for the ν(Ir–CO) normal mode. For comparison, a value of $S = 2.7$ ($\Delta Q = 0.15$ Å) was extracted from fits to the ν(M–CO) vibronic structure of the $^1A_{1g} \rightarrow {}^1T_{1u}$ MLCT transition of $W(CO)_6$ in an argon matrix at 10 K.[17] Since distortion along the ν(M–CO) normal coordinate[18] is considerably smaller for bands C and D of the $Ir_2(\mu\text{-pz})_2(CO)_4$ compounds, these excitations are concluded to have less MLCT character than the transition to $^1T_{1u}$ in $W(CO)_6$.

The absence of resolved ν(Ir–CO) vibronic structure in bands A and B may be attributable to the large distortions of the $^{1,3}B_1$ excited states along the $\nu(Ir_2)$ coordinate,[1] which might obscure short progressions in ν(Ir–CO). It is still puzzling, however, that vibronic structure in ν(M–CO) has not been reported for the absorption spectra of monomer analogues,[10] whereas it is clearly resolved for bands C and D of these dimers even at room temperature (Figure 2). A possible explanation is that the covalent Ir_2 interaction in the $^{1,3}B_1$ excited states may lead to an effective decoupling of π^*(CO) and p_z(Ir) in these states. Thus, the MLCT character of the coupled-monomer excitations could end up being concentrated in the $^{1,3}A_1$ states, thereby giving them higher MLCT character than the monomer excited states. In order to test this hypothesis, however, the electronic spectra of some representative monomers (such as those of Table I) need to be examined at high resolution so as to establish their excited-state distortions along metal–ligand stretching coordinates and determine how they compare to those determined for the $^{1,3}A_1$ excited states of the $Ir_2(\mu\text{-pz})_2(CO)_4$ compounds.

Acknowledgment. We thank L. S. Fox for helpful discussions and for donating the sample of compound **1** that was used for the polarized emission experiments. This work was supported by the National Science Foundation.

(16) Miskowski, V. M.; Albin, M.; Hopkins, M. D.; Brinza, D. E.; Gray, H. B. *Comput. Chem.* **1988**, *12*, 171–174.
(17) Trogler, W. C.; Desjardins, S. R.; Solomon, E. I. *Inorg. Chem.* **1979**, *18*, 2131–2136.
(18) ΔQ as given in the text is for the normal mode and requires further manipulation to give the changes in individual M–CO bond distances. For $W(CO)_6$, the approximate prescription is to divide by the square root of 6. For the title compounds, a normal-coordinate analysis would be required.